Particulate reduction in ternary-compound film growth via pulsed laser deposition from segmented binary-targets

James A Grant-Jacob,* Jake J. Prentice, Stephen J. Beecher, David P. Shepherd, Robert W. Eason and Jacob I. Mackenzie
[1] Optoelectronics Research Centre, University of Southampton, Southampton, SO17 1BJ, UK

E-mail: J.A.Grant-Jacob@soton.ac.uk

Abstract. We present the hetero-epitaxial growth of high-quality crystalline $Y_3Ga_5O_{12}$ onto a <100>-oriented YAG substrate via pulsed laser deposition, using mixed ternary-compound and segmented binary-compound targets. We observe that a $Y_3Ga_5O_{12}$ film fabricated using a segmented target (Y_2O_3/Ga_2O_3) contained ~ 100 times fewer scattering points than a film grown using a mixed $Y_3Ga_5O_{12}$ target. We show that following ablation, the surface of the mixed compound (ternary) target had laser-induced cone structures, whereas the surface of single compound (binary) targets did not. It is concluded that the different ablation dynamics of the oxide constituents in the respective targets plays a significant role in the origin of the scattering points in the resultant films.

Keywords: pulsed laser deposition, crystal structure, laser ablation, surface structure, thin films, ceramic target

PACS codes: 81.15.Fg; 79.20.Eb; 81.15.Fg; 81.15.Fg; 85.70.Ge.

1. Introduction

Pulsed Laser Deposition (PLD) is a simple and versatile technique that uses laser pulses to deposit a wide range of materials such as metals [1], ferromagnetic materials [2], chalcogenides [3], oxides [4], and, as discussed here, laser host materials such as garnets that are often of a ternary or quaternary composition [5–7]. In PLD, laser pulses are incident on a target material, causing rapid heating and subsequent ablation, in which electrons, atoms, ions, molecules, clusters and particles, are ejected from the target as a plasma plume. The plume expands as it propagates toward a substrate, which is usually heated and positioned at an appropriate distance of a few cm from the target, where some of the ejected matter is deposited. Repetitive ablation of the target material therefore allows the growth of a crystalline film, at rates that we have observed can approach 20 μm per hour [8].

The thickness, uniformity and composition (stoichiometry, degree of crystallinity) of a grown film is dependent on PLD parameters that include the laser repetition rate, fluence and pulse length, the choice of background gas and pressure, substrate temperature, target-substrate distance, and target composition [9–15]. Targets are most frequently in the form of a ceramic disc fabricated from compression and sintering of a powdered version of the material intended for growth and therefore comprise single binary compounds (e.g. Y_2O_3) or mixed compounds (e.g. Y_2O_3 and Ga_2O_3). Appropriate choices in the atomic ratio of the constituents is required for growing a stoichiometric film (e.g. $Y_3Ga_5O_{12}$ (YGG)).

The target dimensions are typically much larger than the area ablated by the incident laser beam, and so in order to optimally utilize the available surface area, targets are generally rotated [16], and/or the laser is raster-scanned over the target's surface [17]. It is very important to limit the number of pulses incident on the same target location in order to minimise surface degradation, which occurs due to repetitive ablation, and can result in the formation of cones or other undesirable surface structuring that becomes progressively more pronounced with an increasing number of pulses [18]. These cones are observed to point back along the propagation axis of the incident laser beam, as demonstrated in the schematic in Figure 1. The formation mechanism for these cones can be due to a range of laser-material interaction processes and has sparked much debate over the past 30 years of PLD research [19–21]. However, one clear reason for this effect is inhomogeneity of the target's surface, due to either the initial surface quality during its manufacture or as a result of re-conditioning, or as discussed in this work, the inherent target composition and granular structure as a mix of constituent powders.

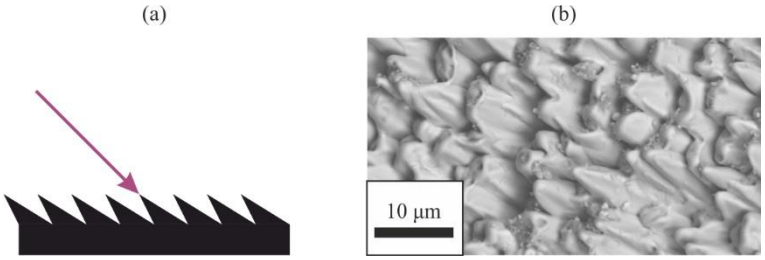

Figure 1. a) Diagram of the cross-section of surface structure caused by laser ablation, showing formation of cones with their vertex orientated toward the incident laser beam. b) Secondary-electron microscope image of cones on the surface of an ablated target formed from its constituent powders of Y_2O_3 and Ga_2O_3.

A consequence of the presence of these cones is that they can progressively reduce the efficiency of ablation [18,22], due to their geometry with respect to the incident laser pulse direction. They also contribute to an increase in particulates ejected from the target [23], whereby the tip of a cone can be ejected and become incorporated into the film growing on the substrate. Such particulates are undesirable in single-crystal films used as optical waveguides, since they can be a source of scattering points and contribute to propagation losses. Optical loss in active and passive waveguide devices leads to a degradation in performance [24].

In this work, for purposes of direct comparison, we show that a crystalline YGG film, deposited using a target consisting of two separate segments of Y_2O_3 and Ga_2O_3, had a markedly reduced particulate count compared to a crystalline YGG film fabricated from a target of mixed Y_2O_3 and Ga_2O_3 composition. We also show that when binary compound, Y_2O_3 and Ga_2O_3, targets were ablated during PLD, no cones were formed on their surface. However, when a target comprised of mixed powders of Y_2O_3 and Ga_2O_3 was ablated under the same conditions, cones on the target surface were readily formed.

2. Experimental procedure

2.1. *Experimental setup*

In the PLD setup used in this work (see schematic in figure 2), pulses of ~ 20-ns duration and wavelength of 248 nm (UV) produced from a KrF excimer laser operating at a repetition rate of 20 Hz, were focused into a stainless steel vacuum chamber, which was back-filled with oxygen to a pressure of 2×10^{-2} mbar. Inside the chamber, the laser beam was focused to produce a fluence of ~ 1 J cm^{-2} on the surface the ceramic-disc target (50-mm in diameter and 5-mm thick), which was rotated, using a DC motor, on a cam introducing an epitroichoidal path for the incident laser beam. Such a motion produced an ablation ring of ~ 12-mm in width and ~ 45-mm outer diameter, after many thousands of shots, and was designed to enable greater target utilization during deposition. Targets consisting of a mixture of nominally three-eighths Y_2O_3 and five-eighths Ga_2O_3 (referred to as the *mixed* YGG), and a disc comprising two spatial segments of three-eighths Y_2O_3 and five-eighths Ga_2O_3 (referred to as *segmented* YGG), were used for the deposition of the thin films.

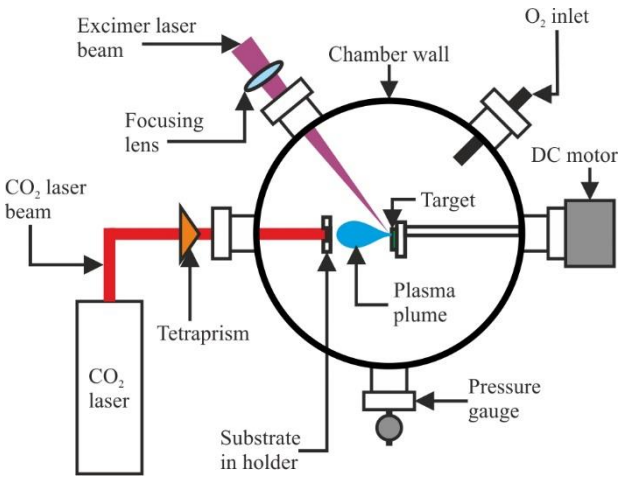

Figure 2. Schematic of pulsed laser deposition setup.

The laser ablation plume was incident on the surface of a 10-mm×10-mm×1-mm <100>-orientated YAG substrate that was polished on both faces. To ensure uniformity of the deposited film over the whole substrate, homogenous heating of the substrate was carried out using a CO_2 laser (10.6 μm wavelength, maximum output of 38 W). The CO_2 laser beam was spatially re-formatted using a tetrapism to produce a square 'top-hat' intensity profile on the rear-face of the substrate [12]. To minimize heat sinking and to maintain the homogeneity of the heating, the substrate was held using an alumina cradle with minimal surface contact. Specifically, an incident CO_2 laser power of 10.5 W – 14 W, heated the substrate to ~ 700 °C – 760 °C, estimated from previous calibration experiments in which metal foils of known melting point were attached to the substrate [25].

2.2. *Target fabrication and deployment*

The mixed YGG target was fabricated from compression and sintering of powders in the 3:5 atomic percentage ratio of Y_2O_3 to Ga_2O_3, which had an average particle size of ~ 11.4 μm for Y_2O_3 and ~ 1.9 μm for Ga_2O_3, from the data supplied by the target manufacturer. The segmented YGG target was formed from two binary targets, cut and shaped using a diamond tipped Dremel® rotary saw and reassembled to the normal circular 50-mm diameter format. Although it was expected that imperfect ablation would occur at the rough edge of the join between the two target pieces, this area was only ~1/500 of the total area of the re-assembled target. Thus it was considered that the contribution to particulates from his region would be negligible. Such segmented targets have been used previously in PLD experiments, but for an alternative end goal of achieving stoichiometric growth [26,27].

Although it would be preferable to be able to change the ablation laser pulse energy on a segment-to-segment basis in order to use the optimal ablation fluence for each target segment (i.e. the fluence that produced lowest scattering points in the grown films for each material), in our setup this was not achievable. Thus, a laser ablation fluence of ~ 1 J cm^{-2} was chosen for the deposition using a segmented target, since this was also the fluence used for ablation of the mixed YGG target. Based on earlier work [28], which analysed sequential PLD growth using two physically different targets in a multi-beam PLD deposition system, it was necessary to keep the maximum number of pulses for each segment below 50 (layer thickness ~ 1 nm). This avoided growth of discrete multilayers of Y_2O_3 and Ga_2O_3 that can occur if sequential ablation occurs involving too many laser pulses per segment. Since the rotation speed of the target in our setup was 1 revolution per second, 20 pulses were incident on the target in one rotation, which meant that for each rotation of the segmented target, there were significantly fewer than 50 pulses per segment, thus allowing for the growth of a crystalline YGG film.

2.3. *Material characterisation*

For each deposition, the corresponding target was ablated using a total of 36,000 pulses, which produced ~ 2-μm thick films. The YGG films were analysed using a dark-field microscope (Nikon L200D) to determine the number of scattering points and the crystalline quality was evaluated via X-ray diffraction

(XRD) using a Rigaku Smartlab X-ray diffractometer. The targets were analysed using a scanning electron microscope (SEM) (Zeiss Evo 50) to characterize their surface topology.

3. Results and discussion

3.1. *Thin film quality*

The XRD spectra of the film grown from the mixed YGG target is shown in figure 3 (green dotted-line), along with the XRD spectra for the YGG film grown from the segmented YGG target (green solid-line). The database values for the (400) YGG peak and the (400) YAG substrate peak, are displayed as a black-dashed line and black-dotted line, respectively. It is evident from the plot that crystalline YGG has been faithfully grown using the segmented target, and the (400) YGG peak position value from the film is an exact match to the database value, indicating the film has the correct composition of $Y_3Ga_5O_{12}$. However, the (400) YGG peak position value from the film deposited using the mixed YGG target is lower than that of the database value by a 2θ value of 0.1° at 28.06 ° indicating a reduction of the gallium content within the film [12].

The broader full width at half maximum (FWHM) of the (400) YGG peak from the film grown using a segmented YGG target (0.11°), compared with the FWHM of the (400) YGG peak from the film grown from the mixed YGG target (0.03°) is interesting and warrants some further comment. Unlike the case for ablation from the mixed target, use of a segmented target leads to a sequential or stepwise deposition of elemental Y and Ga (or their oxides) in the growing YGG film. As discussed in section 2.2, previous work suggests that deposition using more than 50 pulses for sequential ablation of two separate targets in a multi-beam chamber can lead to layering of the two target compounds [28]. However, in this work, since a thickness of ~ 0.05 nm of material is deposited per pulse, on average, 12.5 sequential ablation pulses of the Ga_2O_3 segment per target rotation potentially deposits ~ 0.625 nm of Ga_2O_3 oxide, and so layers of Ga_2O_3 are potentially grown in addition to the formation of $Y_3Ga_5O_{12}$, that can be formed following the deposition of the necessary Y_2O_3. Likewise, since, on average, 7.5 ablation pulses hit the Y_2O_3 segment per target rotation, a potential deposition of ~ 0.375 nm of Y_2O_3 may occur, and so layers of Y_2O_3 could also be produced in addition to the formation of $Y_3Ga_5O_{12}$. Such minority phases of Ga_2O_3 and Y_2O_3 can indeed be observed in Fig. 3b), which presents the XRD spectra of film growth from a segmented-target for a 2θ scan range from 42° to 66°, and shows the growth of (202) Ga_2O_3 at a 2θ peak value of 44.1° and a growth of (721) Y_2O_3 at a 2θ peak value of 64.25°. Since the height of these alternative peaks are relatively small compared with the (400) YGG peak (0.3 % and 0.1 % for (202) Ga_2O_3 and (721) Y_2O_3, respectively, normalised to the peak height of the intended $Y_3Ga_5O_{12}$ film growth), they only appear to cause broadening of the (400) YGG peak, as the (400) YGG peak value matches the database value.

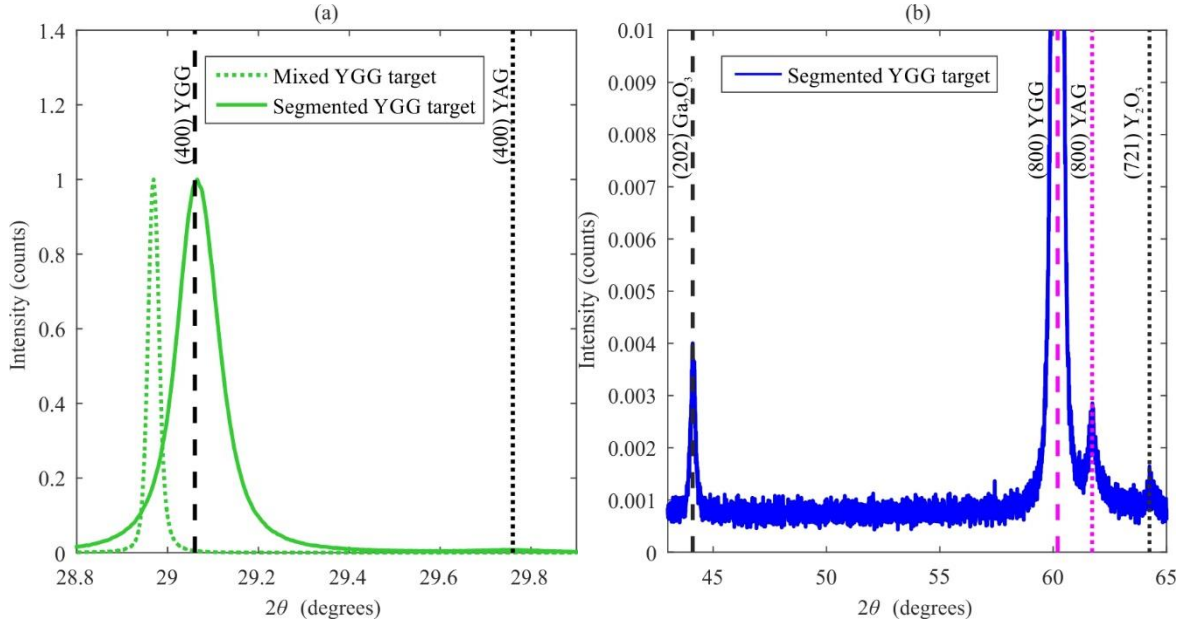

Figure 3. a) XRD spectra of YGG film grown using mixed YGG target (green dotted-line) and segmented YGG target (green solid-line). Black dashed-line indicates (400) YGG database value. Black dotted-line indicates (400) YAG database value. b) XRD spectra of YGG film grown using the segmented YGG target. Black dashed-line indicates (202) Ga_2O_3 database value. Black dotted-line indicates (721) Y_2O_3 database value. Magenta dashed-line indicates (800) YGG database value. Magenta dotted-line indicates (800) YAG database value

Dark-field microscope images of the film deposited from the mixed YGG target and segmented YGG target, taken using a 100-x magnification objective, are shown in figure 4. The white features in the figure are regions of the film from which light has been scattered. Using a peak-intensity detection algorithm, 566 peaks were determined to be present in the image of the thin film grown using a mixed YGG target, while only 5 peaks were detected in the image of the thin film grown using a segmented YGG target.

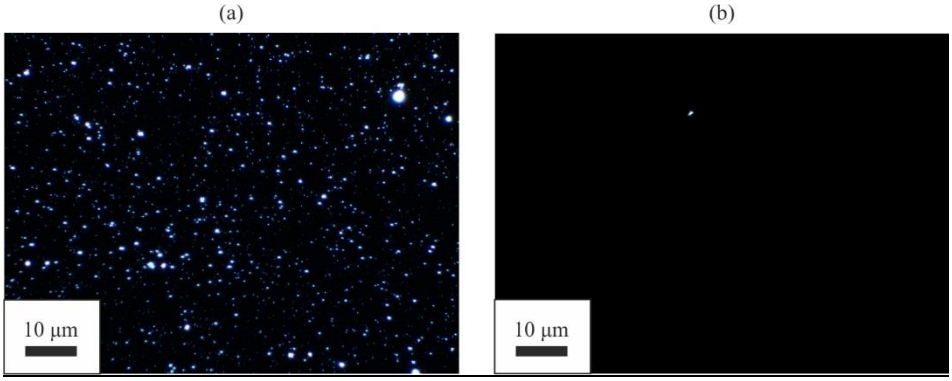

Figure 4. Dark-field microscope image of YGG film grown using a) a mixed YGG target and b) a segmented YGG target, taken using a 100-x magnification objective.

SEM images of the surfaces of the film, displayed in figure 5, show that the scattering points on the surface do appear to be particulates, rather than phase growth, owing to their non-cubic shape.

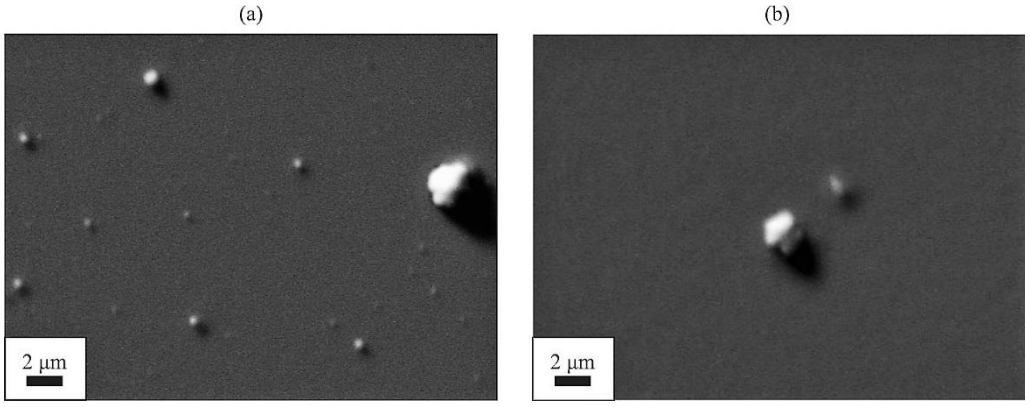

Figure 5. SEM secondary-electron image of the surface of a YGG film grown using a) a mixed YGG target and b) a segmented YGG target.

3.2. *Target surface topology*

To further aid in understanding the differences between the numbers of scattering points within the film grown using the mixed YGG target and the film grown using the segmented YGG target, the surfaces of the targets were analysed before and after ablation. Figure 6 displays SEM secondary-electron images of the surface of the targets before ablation (a-c) and after ablation (d-f). Before ablation, the surface of all the targets look similar, with the structure of the constituent powder present in all. After ablation, the surfaces of Y_2O_3 and Ga_2O_3 show no signs of structure that was present before ablation and no signs of conical structures. However, as seen in figure 6 e), irregular cone-like features of ~ 10-µm diameter are present on the surface of the mixed YGG target.

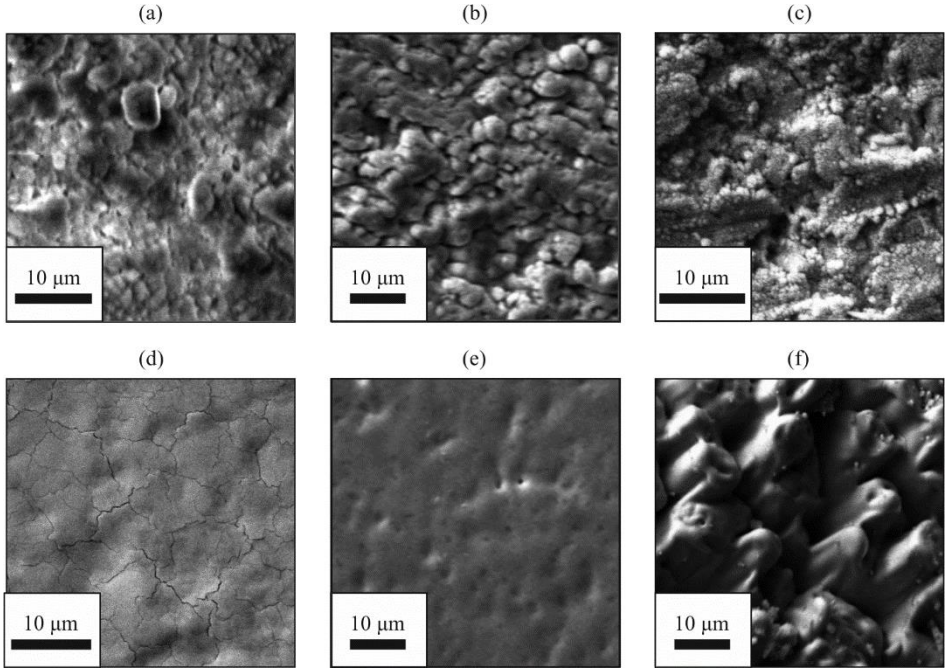

Figure 6. SEM secondary-electron images of the surface of a) Y_2O_3, b) Ga_2O_3 and c) mixed YGG targets before ablation. SEM secondary-electron images of the surface of d) Y_2O_3, e) Ga_2O_3 and f) mixed YGG targets after ablation.

This cone structure is also likely to contribute to the difference in stoichiometry between the two YGG films, indicated in Fig. 3, since the stoichiometry and geometry of these cones can be different to that of non-ablated regions [29–31]. In this instance, this means less Ga is potentially being transferred from the target to the substrate. Since the mixed YGG target was formed from a sintered hot-pressed combination of two materials Y_2O_3 and Ga_2O_3, the surface of the target will inevitably possess non-uniformity of composition that results from the intrinsic particle size of the grains from which the target is formed.

Within the mixed YGG target, the different ablation thresholds of each of the binary compounds, which results from their differing values of optical absorption, thermal conductivity, melting and boiling points (e.g. Ga_2O_3 and Y_2O_3 melting points are 1900 ^oC and 2425 ^oC, respectively), combined with the non-homogenous initial distribution of the compounds within the target, all point to an explanation for the origin of the cone structure on the surface of the mixed YGG target. The higher percentage of porosity of the mixed YGG target, 32.1 %, compared with the segmented targets, which were 19.4 % and 16.6 %, for Y_2O_3 and Ga_2O_3, respectively, potentially contributed to the higher particulates present in the films. Although the cones can progressively reduce the efficiency of ablation, in this work, the relatively few pulses-per-site, (~ 240 pulses-per-site) was found to not decrease the deposition rate significantly. In work by others, it has been found for the PLD of $YBa_2Cu_3O_{7-x}$, by 2000 pulses-per-site, ablation rate of 10 % initial rate can be reached [18].

The correlation between the presence of cones on the target and a significantly higher (by a factor of ~ 100) number of scattering points when using the mixed target compared to a segmented target suggests an obvious way forward for future PLD growth strategies, if reduced particulate counts are an important factor for the particular PLD research direction. The effect of target surface quality with variation in deposition parameters, such as fluence, has been explored by O'Brien et al. [32], in which higher fluence increased the angle of the cone slant height relative to the surface of the target and increased the particle density in the grown film. However, future work should involve analysis of the chemical composition of the particulates in the film to clarify any potential variation in the origin of the target particulates over the surface of the film.

4. Conclusion

We have examined the fabrication of crystalline YGG on a <100>-orientated YAG substrate via PLD, using a mixed compound YGG target as well as a segmented target consisting of Y_2O_3 and Ga_2O_3 sectors. Our results show that a crystalline film grown using a segmented target produced ~ 100x fewer particulates than a film grown using a mixed target. We have shown that for Y_2O_3 and Ga_2O_3 segments, no evident periodic surface structuring was present after ablation, while for a mixed compound YGG target, cone-like structures were created. Our results demonstrate the ability to reduce the number of particulates in the grown films, whose origin is associated with the presence of cone structures on the surface of mixed compound targets.

Acknowledgements

The authors acknowledge the support of the EPSRC through grant numbers EP/N018281/1 and NASA grant number GSFC NNG15HQ01C. The RDM data for this paper can be found at DOI: 10.5258/SOTON/D0333.

References

[1] J.G. Lunney, Pulsed laser deposition of metal and metal multilayer films, Appl. Surf. Sci. 86 (1995) 79–85.

[2] A. Sposito, G.B.G. Stenning, S.A. Gregory, P.A.J. de Groot, R.W. Eason, Compositional tuning of yttrium iron garnet film properties by multi-beam pulsed laser deposition, Thin Solid Films. 568 (2014) 31–37.

[3] A. V Rode, A. Zakery, M. Samoc, R.B. Charters, E.G. Gamaly, B. Luther-Davies, Laser-deposited As_2S_3 chalcogenide films for waveguide applications, Appl. Surf. Sci. 197 (2002) 481–485.

[4] R. Guo, L. You, M. Motapothula, Z. Zhang, M.B.H. Breese, L. Chen, D. Wu, J. Wang, Influence of target composition and deposition temperature on the domain structure of $BiFeO_3$ thin films, AIP Adv. 2 (2012) 42104.

[5] J.A. Grant-Jacob, S.J. Beecher, T.L. Parsonage, P. Hua, J.I. Mackenzie, D.P. Shepherd, R.W. Eason, An 11.5 W Yb:YAG planar waveguide laser fabricated via pulsed laser deposition, Opt. Mater. Express. 6 (2016) 91–96.

[6] T.L. Parsonage, S.J. Beecher, A. Choudhary, J.A. Grant-Jacob, P. Hua, J.I. Mackenzie, D.P. Shepherd, R.W. Eason, Pulsed laser deposited diode-pumped 74 W Yb:Lu_2O_3 planar waveguide laser, Opt. Express. 23 (2015) 31691.

[7] S.J. Beecher, J.A. Grant-Jacob, P. Hua, J.J. Prentice, R.W. Eason, D.P. Shepherd, J.I. Mackenzie, Ytterbium-doped-garnet crystal waveguide lasers grown by pulsed laser deposition, Opt. Mater. Express. 7 (2017) 1628–1633.

[8] J.A. Grant-Jacob, S.J. Beecher, D.P. Shepherd, R.W. Eason, J.I. Mackenzie, Pulsed laser deposition of garnets at a growth rate of 20-microns per hour, in: E-MRS 2017 Spring Meet., Strasbourg, France, 2017: p. Q 1.9.

[9] R.W. Eason, T.C. May-Smith, C. Grivas, M.S.B. Darby, D.P. Shepherd, R. Gazia, Current state-of-the-art of pulsed laser deposition of optical waveguide structures: Existing capabilities and future trends, Appl. Surf. Sci. 255 (2009) 5199–5205.

[10] P.R. Willmott, J.R. Huber, Pulsed laser vaporization and deposition, Rev. Mod. Phys. 72 (2000) 315.

[11] R. Castro-Rodriguez, D.R. Coronado, A. Iribarren, B.E. Watts, F. Leccabue, J.L. Pena, Correlation between target--substrate distance and oxygen pressure in pulsed laser deposition of complex oxide thin films, Appl. Phys. A. 81 (2005) 1503–1507.

[12] J.I. Mackenzie, J.A. Grant-Jacob, S. Beecher, H. Riris, A.W. Yu, D.P. Shepherd, R.W. Eason, Er:YGG planar waveguides grown by pulsed laser deposition for LIDAR applications, in:

W.A. Clarkson, R.K. Shori (Eds.), Proc. SPIE, SPIE, San Francisco, United States, 2017: p. 100820A.

[13] J.A. Grant-Jacob, S.J. Beecher, T.L. Parsonage, P. Hua, J.I. Mackenzie, D.P. Shepherd, R.W. Eason, Engineering of thin crystal layers grown by pulsed laser deposition, in: J.I. Mackenzie, H. JelÍnková, T. Taira, M. Abdou Ahmed (Eds.), Proc. SPIE 9893, Laser Sources Appl. III, SPIE, Brussels, Belgium, 2016: p. 98930E.

[14] A. Sambri, D. V Cristensen, F. Trier, Y.Z. Chen, S. Amoruso, N. Pryds, R. Bruzzese, X. Wang, Plasma plume effects on the conductivity of amorphous-$LaAlO_3/SrTiO_3$ interfaces grown by pulsed laser deposition in O_2 and Ar, Appl. Phys. Lett. 100 (2012) 231605.

[15] J.A. Grant-Jacob, S. J. Beecher, H. Riris, A. Yu, D. Shepherd, R. Eason, J. Mackenzie, Dynamic control of refractive index during pulsed laser deposited waveguide growth, Opt. Mater. Express. 7 (2017) 4073–4081.

[16] C. Doughty, A.T. Findikoglu, T. Venkatesan, Steady state pulsed laser deposition target scanning for improved plume stability and reduced particle density, Appl. Phys. Lett. 66 (1995) 1276–1278.

[17] J.A. Greer, History and current status of commercial pulsed laser deposition equipment, J. Phys. D Appl. Phys. 47 (2014) 34005.

[18] S.R. Foltyn, R.C. Dye, K.C. Ott, E. Peterson, K.M. Hubbard, W. Hutchinson, R.E. Muenchausen, R.C. Estler, X.D. Wu, Target modification in the excimer laser deposition of $YBa_2Cu_3O_{7-x}$ thin films, Appl. Phys. Lett. 59 (1991) 594–596.

[19] P.E. Dyer, S.D. Jenkins, J. Sidhu, Development and origin of conical structures on XeCl laser ablated polyimide, Appl. Phys. Lett. 49 (1986) 453–455.

[20] L.K. Ang, Y.Y. Lau, R.M. Gilgenbach, H.L. Spindler, J.S. Lash, S.D. Kovaleski, Surface instability of multipulse laser ablation on a metallic target, J. Appl. Phys. 83 (1998) 4466–4471.

[21] H.M. Christen, G. Eres, Recent advances in pulsed-laser deposition of complex oxides, J. Phys. Condens. Matter. 20 (2008) 264005.

[22] N.B. Ibrahim, C. Edwards, S.B. Palmer, Pulsed laser ablation deposition of yttrium iron garnet and cerium-substituted YIG films, 220 (2000) 183–194.

[23] H.L. Spindler, R.M. Gilgenbach, J.S. Lash, Effects of laser-ablation target damage on particulate production investigated by laser scattering with deposited thin film and target analysis, Appl. Phys. Lett. 68 (1996) 3245–3247.

[24] S.J. Barrington, T. Bhutta, D.P. Shepherd, R.W. Eason, The effect of particulate density on performance of Nd:$Gd_3Ga_5O_{12}$ waveguide lasers grown by pulsed laser deposition, Opt. Commun. 185 (2000) 145–152.

[25] A. Sposito, Pulsed laser deposition of thin film magneto-optic materials and lasing waveguides, University of Southampton, 2014.

[26] H.-M. Christen, D.P. Norton, L.A. Géa, L.A. Boatner, Pulsed laser deposition of solid-solution films using segmented targets, Thin Solid Films. 312 (1998) 156–159.

[27] S. Yilmaz, T. Venkatesan, R. Gerhard-Multhaupt, Pulsed laser deposition of stoichiometric potassium-tantalate-niobate films from segmented evaporation targets, Appl. Phys. Lett. 58 (1991) 2479–2481.

[28] K.A. Sloyan, T.C. May-Smith, M. Zervas, R.W. Eason, S. Huband, D. Walker, P. a Thomas, Growth of crystalline garnet mixed films, superlattices and multilayers for optical applications via shuttered combinatorial pulsed laser deposition., Opt. Express. 18 (2010) 24679–24687.

[29] X.Y. Chen, Z.G. Liu, Interaction between laser beam and target in pulsed laser deposition: laser fluence and ambient gas effects, Appl. Phys. A Mater. Sci. Process. 69 (1999) S523--S525.

[30] E. Morintale, C. Constantinescu, M. Dinescu, Thin films development by pulsed laser-assisted deposition, Phys. AUC. 20 (2010) 43–56.

[31] V. Tsaneva, R. Tomov, D. Ouzounov, T. Donchev, Influence of cumulative laser irradiation on YBCO thin film pulsed laser deposition, Czechoslov. J. Phys. 46 (1996) 1529–1530.

[32] T.P. O'Brien, J.F. Lawler, J.G. Lunney, W.J. Blau, The effect of laser fluence on the ablation and deposition of $YBa_2Cu_3O_7$, Mater. Sci. Eng. B. 13 (1992) 9–13.